Applying the polarization memory effect in polarization-gated subsurface imaging

Ralph Nothdurft and Gang Yao

Department of Biological Engineering, University of Missouri-Columbia, Columbia, MO 65211
renothdurft@mizzou.edu, yaog@missouri.edu

Abstract: Polarization memory is a well established phenomenon occurring when circularly polarized light propagates in turbid media of larger particles. Recent studies have demonstrated that the circularly cross-polarized imaging can significantly improve subsurface reflection contrast due to the polarization memory effect. We have found that such improvement is strongly influenced by the optical properties of the media. Circularly cross-polarized light provides superior image enhancement in low scattering media, but becomes inferior in high scattering media. Our experiments also demonstrate that polarization imaging provides no significant improvement to image resolution.

OCIS codes: (260.5430) Polarization; (290.1350) Backscattering; (110.7050) Turbid media; (170.0110) Imaging system.

References and links

1. S. G. Demos and R. R. Alfano, "Optical polarization imaging," Appl. Opt. **36**, 150–155 (1997).
2. G. D. Lewis, D. L. Jordan, and P. J. Roberts, "Backscattering target detection in a turbid medium by polarization discrimination," Appl. Opt. **38**, 3937–3944 (1999).
3. S. G. Demos, H. B. Radousky, and R. R. Alfano, "Deep subsurface imaging in tissues using spectral and polarization filtering," Opt. Express **7,** 23–28 (2000).
4. S. Morgan and I. Stockford, "Surface-reflection elimination in polarization imaging of superficial tissue," Opt. Lett. **28**, 114–116 (2003).
5. J. S. Tyo, M. P. Rowe, E. N. Pugh, Jr., and N. Engheta, "Target detection in optically scattered media by polarization-difference imaging," Appl. Opt. **35**, 1855–1870 (1996).
6. S. L. Jacques, J. R. Roman, and K. Lee, "Imaging superficial tissues with polarized light", Lasers Surg. Med. **26**, 119–129 (2000).
7. J. G. Walker, P. C. Y. Chang, and K. I. Hopcraft, "Visibility depth improvement in active polarization imaging in scattering media," Appl. Opt. **39**, 4933–4941 (2000).
8. P. C. Y. Chang, J. C. Flitton, K. I. Hopcraft, E. Jakeman, D. L. Jordan, and J. G. Walker, "Improving visibility depth in passive underwater imaging by use of polarization," Appl. Opt. **42**, 2794–2803 (2003).
9. G. Yao and L.-H. Wang, "Propagation of polarized light in turbid media: an animated-simulation study," Opt. Express **7**, 198–203 (2000).
10. F. C. MacKintosh, J. X. Zhu, D. J. Pine, and D. A. Weitz, "Polarization memory of multiply scattered light," Phys. Rev. B **40**, 9342–9345 (1989).
11. A. D. Kim and M. Moscoso, "Backscattering of circularly polarized pulses," Opt. Lett. **27**, 1589–1991 (2002).
12. X. Ni and R. R. Alfano, "Time-resolved backscattering of circularly and linearly polarized light in a turbid medium," Opt. Lett. **29**, 2773–2775 (2004).
13. S. A. Kartazayeva, Xiaohui Ni, and R. R. Alfano, "Backscattering target detection in a turbid medium by use of circularly and linearly polarized light," Opt. Lett. **30**, 1168–1170 (2005).
14. R. Nothdurft and G. Yao, "Expression of target optical properties in subsurface polarization-gated imaging," Opt. Express **13**, 4185-4195 (2005).
15. X. Ma, J. Q. Lu, R. S. Brock, K. M. Jacobs, P. Yang, and X. Hu, "Determination of complex refractive index of polystyrene microspheres from 370 to 1610 nm," Phys. Med. Biol. **48**, 4165–4172 (2003).
16. G. Yao, "Differential optical polarization imaging in turbid media with different embedded objects," Opt. Comm. **241**, 255–261 (2004).
17. R. Nothdurft and G. Yao, "Effects of turbid media optical properties on object visibility in subsurface polarization imaging," Appl. Opt. In press (2006).
18. A. H. Hielscher, A. A. Eick, J. R. Mourant, D. Shen, J. P. Freyer, and I. J. Bigio, "Diffuse backscattering Mueller matrices of highly scattering media," Opt. Express **1**, 441–453 (1997).

#68105 - $15.00 USD Received 15 February 2006; revised 9 May 2006; accepted 12 May 2006

1. Introduction

Polarization imaging has shown potential for revealing otherwise hidden objects embedded in highly scattering media [1−8]. In addition to various processing methods [5−8] for image contrast enhancement, there are special interests in exploring the different propagation properties of linearly and circularly polarized light in scattering media [9]. In turbid media of larger scattering particles, previous studies have shown that circularly polarized light tends to maintain its original polarization state [10−12] even when the polarization state of linearly polarized incident light is randomized. This effect, termed "polarization memory," results from the increased propensity for small-angle forward scattering in the media coupled with a tendency of forward scattering to preserve helicity. Very recently it has been demonstrated [12, 13] that as a result, circularly polarized light, specifically the circularly cross-polarized component, can significantly improve image contrast. It still remains a question however, as to whether a specific polarization component can be universally applied and to what extent polarization memory can be useful.

In this study, we show that polarization memory effect on subsurface imaging visibility can vary dramatically with the optical properties of the turbid media. The circularly cross-polarized light may provide superior image enhancement in one sample, and become inferior in another. Our experiments also indicate that although polarization imaging can improve image visibility under certain experimental conditions, it is insignificant in improving image resolution.

2. Materials and methods

We used the same imaging configuration (Fig. 1) as in our previous investigation [14]. A polarized 633 nm laser was expanded to a collimated beam 2 cm in diameter and strikes the target at 45º incidence. Returning light was measured by a CCD camera normal to the surface of the scattering medium. Polarization states were controlled by a variable waveplate prior to the sample and a quarter waveplate and linear polarizer in front of the camera. The measured extinction ratios for both linearly and circularly polarized light exceed 0.05%. Multiple averaging was applied to remove laser speckle. Camera gain was set to the lowest possible setting and the shutter-speed was chosen to maximize the dynamic range, these settings were held constant throughout the investigation. We normalized the images against a field with no target present to remove illumination artifacts.

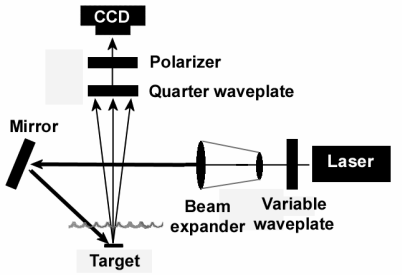

Fig. 1. Schematic diagram of the experimental setup. The target is a small square shaped reflective object submerged in a semi-infinite scattering medium.

Our experimental samples or "phantoms" were constructed by submerging small targets into scattering media. Our background scattering media were made from polystyrene microspheres (Polysciences, Warrington, PA) of different sizes and concentrations. The anisotropy, g, and scattering coefficient, μ_s, were calculated using Mie theory, previously shown to match experimental results [15]. Spheres with 0.989, 0.535, and 0.356 μm diameters were chosen to yield g values of 0.918, 0.839, and 0.722 respectively. Our target was a 3×3 mm^2 square portion of coverslip sputter-coated with a 120 nm layer of platinum. The target was placed on a transparent glass sheet and lowered in 0.2 mm increments via a vertical stage. Tests indicated the glass sheet did not measurably influence the measurements. Zero depth

#68105 - $15.00 USD Received 15 February 2006; revised 9 May 2006; accepted 12 May 2006

was measured relative to the medium surface and was the predominant source of error owing to variation amongst the phantoms and human judgment. Values reported here are reliable within the step size (0.2 mm) of the depth adjustment.

Samples with the same scattering coefficient μ_s but different g values lead to significantly different visibilities in the unpolarized image. The 1st column in Fig. 2 demonstrates that samples with larger anisotropy (or smaller μ_s') have much better unpolarized contrast than samples of smaller anisotropy. We chose to compare phantoms with the same reduced scattering coefficient, $\mu_s' = \mu_s(1-g)$ because we found phantoms with the same μ_s' present nearly identical unpolarized visibility despite variations in g (2nd, 3rd, 4th columns in Fig. 2). This consistent unpolarized behavior provides a reliable reference for examining the effectiveness of polarization detection.

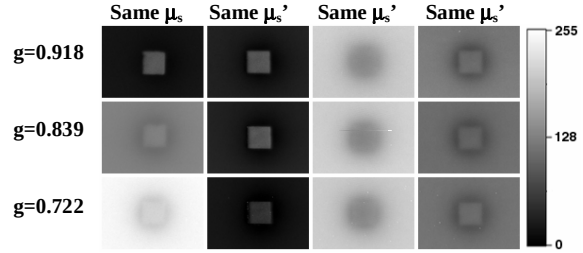

Fig. 2. Unpolarized images of various phantoms used in the study. Rows from top to bottom represent phantoms of 0.989, 0.535, 0.356μm microspheres. Columns from left to right represent phantoms of (1) $\mu_s = 50$, $\mu_a = 0.1$ (2) $\mu_s' = 3.75$, $\mu_a = 0.1$ (3) $\mu_s' = 15$, $\mu_a = 0.1$ (4) $\mu_s' = 15$, $\mu_a = 0.4$. All units are in cm^{-1}. Targets are located at 0.8 mm below surface.

Image visibility was measured using $\left|\overline{T} - \overline{B}\right| / \sigma_B$, where $\overline{T}$ and $\overline{B}$ denote the number of photons in the target and background image pixels, respectively; and σ_B is the standard deviation of the background intensity. The target region, T, was measured from the middle quarter of the target, while the background region, B, comprised the equivalent area split across the four corners of the image. σ_B provides an estimation of the image noise which ultimately determines the target visibility. Pixel values variations in acquired images can be induced by many sources, such as: electronic noise, residual speckle noise, laser power fluctuation, and quantum noise, etc. Such variations are signified in polarization imaging when algebra subtractions are performed to calculate the differential polarization image [3] and the polarization degree image [4]. Considering a simple example where two images have the same mean target and background pixel values but the standard deviation of the background is different. The target stands out better in the image with lower background noise. For pure illumination-based raw polarization component images, however, the new definition produces similar results (with a coefficient difference) as the traditional contrast calculation [14] because standard deviation is found to correlate with pixel intensities in our study. Nevertheless, we found this signal-to-noise (SNR) measurement provides a very good match to visual examination in general polarization imaging system.

To simplify phantom comparison we have used the relative visibility, which simply denotes the ratio of a given polarization image's visibility to that of the unpolarized image. Image resolution is the other critical parameter. The resolution of a single target was calculated by taking the first derivative of the mean line across the target and measuring the full width at half maximum (FWHM) of the distribution on each edge of the object. First derivatives were notoriously noisy and require smoothing using low pass filters. Both visibility and resolution are presented as a function of transport mean free path depth, calculated as $mfp' = 1/(\mu_a+\mu_s')$.

3. Results

Our first experiment involved phantoms with a reduced scattering coefficient μ_s' of $3.75cm^{-1}$ and absorption coefficient μ_a of $0.1\ cm^{-1}$. All three phantoms, consisting of different sized

#68105 - $15.00 USD Received 15 February 2006; revised 9 May 2006; accepted 12 May 2006

particles, reveal nearly identical unpolarized visibility as made evident in the second column of Fig. 2. The reflective target appears bright in the unpolarized image (2nd column in Fig. 2) in comparison with the background medium.

Figure 3 shows the resulting visibility for linear and circular polarized components at different target depths. The dotted line in Fig. 3 at 1.0 relative visibility indicates the matched performance of unpolarized imaging. A surface effect is present at the first few points where the influence of μ_s dominates μ_s'. Beyond this the linear components fall into the same path with the linear co-polarized (CO) component consistently superior to the linear cross-polarized (CR) component. With circular polarization imaging, the CR component is superior owing to reversed helicity from the target surface. If reversed helicity alone was responsible we would expect the three phantoms to follow the same path; however there is a clear improvement with increasing anisotropy. At 1mfp', the CR visibility from 0.989 μm phantom (g = 0.918) is more than 50% better than that of the 0.356 μm phantom (g = 0.722).

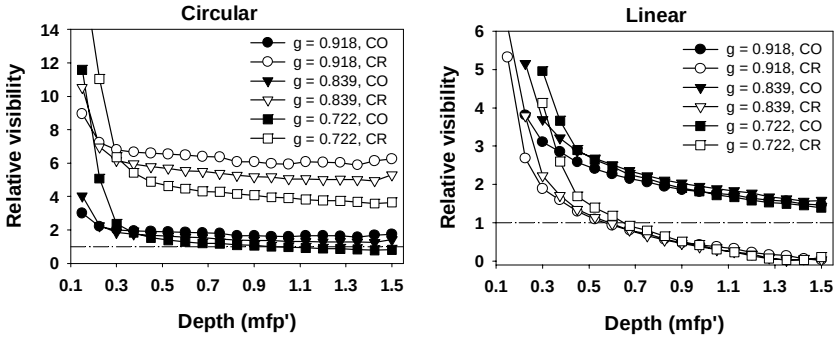

Fig. 3. Image visibility of phantoms with $\mu_s' = 3.75$ cm^{-1} and $\mu_a = 0.1$ cm^{-1}. "CO" indicates co-polarized image, and "CR" refers to cross-polarized image.

Establishing the same reduced scattering coefficient μ_s' with different sized spheres implicitly leads to a different scattering coefficient μ_s in each phantom. The resolution curves shown in Fig. 4 are for phantoms with $\mu_s = 13.49$ cm^{-1} (0.356 μm spheres) and $\mu_s = 45.73$ cm^{-1} (0.989 μm spheres). The curves show that the scattering coefficient μ_s dominates image resolution. At the same reduced scattering coefficient μ_s', phantoms of smaller particles produce images with much better spatial resolution because they have smaller scattering coefficients. For a given phantom the resolution of the best linear and circular component is equivalent to that of the unpolarized image. Thus while polarization memory improves the signal contrast, it has little effect in improving resolution.

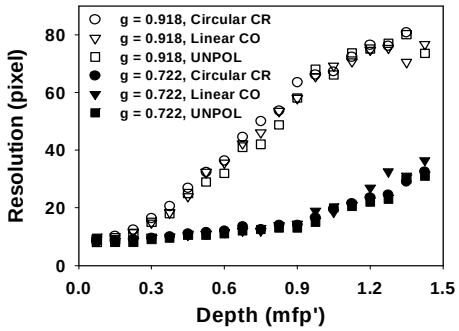

Fig. 4. Image resolution of phantoms with $\mu_s' = 3.75$ cm^{-1} and $\mu_a = 0.1$ cm^{-1}.

In the second experiment we quadrupled the μ_s' of each phantom to 15 cm^{-1} while maintaining the absorption coefficient μ_a at 0.1 cm^{-1}. In all three phantoms the reflective target now appears dark in the unpolarized image at all target depths when comparing with the surrounding medium (see images in the 3rd column of Fig. 2). This radically shifts the

#68105 - $15.00 USD Received 15 February 2006; revised 9 May 2006; accepted 12 May 2006

component visibility as shown in Fig. 5.

The best component for both linear and circular are reversed. Circular CO now demonstrates the best visibility and is slightly better the best linear CR component. It is interesting to note that the circular CR has a minimum around 1mfp′. A close examination reveals that the target appearance in circular CR transitions from bright to dark at this depth. As depth increases circular CR does start to rebound, though only the phantom with the highest g manages to surpass unpolarized light. This might seem to redeem circular CR, but the image visibility is so low after 2.5 mfp′ that the 10% gain is practically insignificant. On the other hand, for the best polarization component CO, polarization memory effect is against its performance. At ~1mfp', the CO visibility from 0.989 μm phantom is ~25% worse than that of the 0.356 μm phantom.

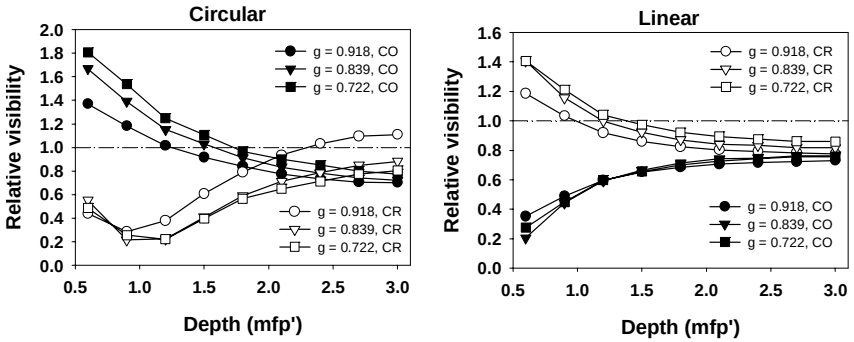

Fig. 5. Image visibility of phantoms with $\mu_s' = 15.0\ cm^{-1}$ and $\mu_a = 0.1\ cm^{-1}$.

Our third experiment increased μ_a to $0.4 cm^{-1}$, restoring the μ_s'/μ_a ratio to that of the first experiment while maintaining a high μ_s'. In the unpolarized images the target appears nearly identical to the background save for a faint surrounding dark halo as shown in the forth column in Fig. 2. This dark halo is generated due to the blocking of diffuse photons by the opaque target used in this study. Although the μ_s'/μ_a ratio has been restored, the components' behavior remains different from the first experiment. The apparent visibility improvement over unpolarized images shown in Fig. 6 is largely due to the unpolarized image being nearly indistinguishable from the background. This also makes the measurements very susceptible to any errors in depth. Nevertheless, circular CO does appear to decline with increasing g as in the second experiment. At around 1mfp′ circular CO surpasses circular CR in all three phantoms. The trend of linear CO shows a minimum at around 1 mfp′, which is similar to how circular CR behaves in the second experiment.

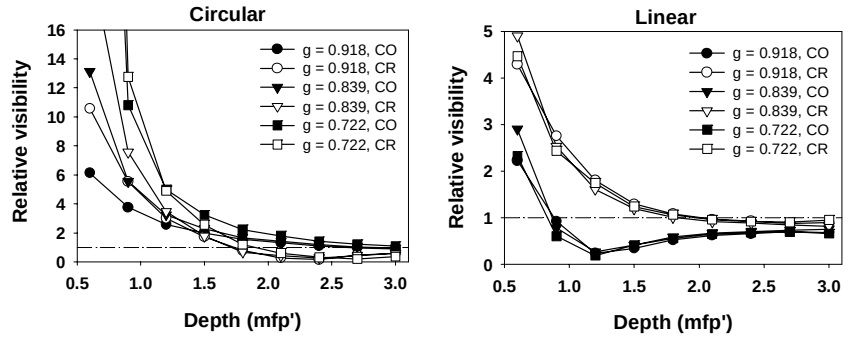

Fig. 6. Image visibility of phantoms with $\mu_s' = 15.0\ cm^{-1}$ and $\mu_a = 0.4\ cm^{-1}$.

4. Discussion

Under the same μ_s', higher g phantoms have higher scattering coefficients which increase the

#68105 - $15.00 USD Received 15 February 2006; revised 9 May 2006; accepted 12 May 2006

chance of depolarization. For each μ_s'/μ_a ratio, a higher g increases circular background co-polarization while depolarizing linear. In phantoms of low μ_s', the polarization memory effects are clear. For linear polarization, the increase in forward scattering simply compensates for the increase in scattering events. By comparison the preservation of helicity afforded to circular polarization by forward scattering overpowers the increased scattering. This is the definitive demonstration of polarization memory effect in imaging. Though we omit the graphs, similar polarization memory effects also appear in the visibility of the degree of polarization (DOP) images [4]. In the high μ_s' phantoms the behavior is more complex. Though there are subtle indications of the influence of polarization memory, the effect is different in the circular CO image, which outperforms circular CR at high μ_s'.

The manner and extent of the image improvement depends largely on the relative weight of information between the target and background. The increase in phantom μ_s' causes a dramatic increase in the back-scattered intensity from the background media while levels from the target remain relatively unchanged. In unpolarized images, the reflective target thus appears as a bright object in the low μ_s' medium (2^{nd} column in Fig. 2), and a dark object in the high μ_s' medium (3^{rd} column in Fig. 2), and each case behaves this way throughout the visible depths. This transition from dark object to bright object significantly changes the relative behavior of the polarization CO and CR components. For circular light in particular, the CO component from the background increases with anisotropy g; where the counterpart circular CR component decreases with g. For a dark target (Fig. 5), a decrease in the background signal reduces visibility; conversely such a change improves the visibility of a bright target (Fig. 3). This combined with reversed helicity explains the disparate polarization memory effects in phantoms of different scattering properties.

Other sample and target properties [16, 17] also play important roles. The background absorption coefficient μ_a has a large impact on highly scattered, and hence highly depolarized, photons. Thus an increase in μ_a changes the behavior of both unpolarized and polarized components. The target reflectance is certainly an essential factor in determining the transition point from a bright target to a dark target. Likewise the transition point should also be influenced by a change in the angle of illumination which also affects the amount of light being detected.

While circularly polarized light can maintain its polarization better under successive small-angle scattering events, it is still dispersed spatially in the same manner as linearly polarized light. This explains why circular light does not improve image resolution in our results. The target's shadow is evident as a dark halo in illumination-based images though this is removed in the DOP image due to its diffuse nature. Although the dark halo (Fig. 2) precludes an accurate measurement of resolution in the component images for high μ_s' phantoms, this behavior in low μ_s' is unambiguous.

5. Conclusion

Visibility under circular polarization was consistently better than linear throughout the investigation, though the best component varied with μ_s'. This improvement did not extend to the resolution of target edges.

The effectiveness of a specific polarization component on improving subsurface imaging depends on the complicated dynamic interactions between the target and background. The effect of polarization memory is strongly influenced by the optical properties of the media and can be helpful only under certain conditions. Our results suggest that caution should be exercised when choosing a specific polarization component in subsurface imaging for visibility improvement. A complete polarization characterization method such as the Mueller matrix measurements [18] may be necessary to ensure desired results. Although only particles of three different sizes were used in this study, our results are applicable to the more general applications of subsurface polarization imaging.

Acknowledgments

This study was supported by a research board grant from University of Missouri-Columbia.

#68105 - $15.00 USD Received 15 February 2006; revised 9 May 2006; accepted 12 May 2006